Research Article

EPR, optical, physical and structural studies of strontium alumino-borate glasses containing Cu^{2+} ions

Mohamad Raheem Ahmed[1] · **Md. Shareefuddin**[2]

Abstract

Glass composition $(30-x)$ SrO–$x$$Al_2O_3$–69.5$B_2O_3$–0.5CuO ($0 \le x \le 15$ mol%) captioned as SABC was prepared by the conventional melt quenching technique. Peak-free X-ray diffractograms and homogeneous plain SEM image confirm the glassy nature of the prepared samples. EPR and optical absorption spectral studies were carried out to understand the effect of modifier oxide (SrO) and transition metal (TM) ion Cu^{2+} in the glass network. From the EPR spectra, spin-Hamiltonian parameters were evaluated. It was observed that $g_{\parallel} > g_{\perp} > g_e$ and $A_{\parallel} > A_{\perp}$ suggest that the ground state of Cu^{2+} is $d_{x^2-y^2}$ ($^2B_{1g}$ state) and the site symmetry around Cu^{2+} is tetragonally distorted octahedral. The optical absorption spectra revealed a broad absorption for all the glass samples. This band is assigned to $^2B_{1g} \rightarrow {}^2B_{2g}$ transition. From optical absorption spectra, optical band gap and Urbach energy values were calculated. The FTIR and Raman spectral studies showed that the glass network consists of BO_3 and BO_4 structural units.

Keywords Borate glasses · Physical · Optical properties · EPR · FTIR · Raman

1 Introduction

Borate is an excellent glass former, and its derived glasses are well known for their high thermal stability, low melting point and good solubility. They find wide application in optical glasses, gamma ray shielding and bioactive materials [1, 2]. Physical and optical properties of borate glasses can be enhanced by the addition of modifiers such as alkali and alkaline earth oxides. In continuation, alkaline earth oxides like SrO-, BaO-, CaO-, MgO-based borate glasses have been prepared and they are being used in various applications such as vacuum ultraviolet (VUV) optics which has the shortest wavelength in the EM spectrum, radiation dosimetry and solar energy converters [3]. Various studies have been conducted to explore the probable physical and optical properties of pure borate glasses added with different modifiers and dopants. Although strontium also plays the main role in biological systems and resembles the calcium element in its properties, like calcium, it is taken up and preferentially located in bones. The ionic size of strontium (Sr^{2+}) is nearly equal to calcium ion (Ca^{2+}) and easily replaceable, and its role in bone metabolism has been reported as well as both anti-resorptive and bone forming for different applications [4, 5]. In addition to this, SrO improves the rigidity of the glass samples and extends its applications in nonlinear optical devices and biological systems [6]. It has been reported that alumino-borate glasses (Al_2O_3–B_2O_3) are refractory compounds possessing excellent physical properties such as low density, high hardness, high Young's modulus, high electrical resistivity and low coefficient of thermal expansion [7]. Abd El-Moneim [8] suggested that ultrasonic velocities and elastic moduli results are purely glass composition dependent and Al_2O_3 acts as network former with Al^{3+} ions by the formation of AlO_4 tetrahedra. From literature survey, Al_2O_3 is a typical intermediate material for borate glasses; it can be changed into either glass network former or modifier controlled by the large or small amount of Al_2O_3, respectively [9]. Al_2O_3 is

✉ Mohamad Raheem Ahmed, mohdraheem1980@gmail.com | [1]Muffakham Jah College of Engineering and Technology, Osmania University, Hyderabad 500034, India. [2]Department of Physics, Osmania University, Hyderabad 500007, India.

SN Applied Sciences (2019) 1:209 | https://doi.org/10.1007/s42452-019-0201-5

Received: 25 September 2018 / Accepted: 21 January 2019 / Published online: 4 February 2019

Table 1 Composition of the $(30-x)SrO–xAl_2O_3–69.5B_2O_3–0.5$ CuO glasses

Glass code	SrO mol%	Al_2O_3 mol%	B_2O_3 mol%	CuO mol%	T_g (°C)
SABC0	25	5	69.5	0.5	613
SABC1	22.5	7.5	69.5	0.5	587
SABC2	20	10	69.5	0.5	584
SABC3	17.5	12.5	69.5	0.5	573
SABC4	15	15	69.5	0.5	561

Fig. 1 Physical appearance of SABC glasses

assumed to enter the structure of $SrO–B_2O_3$ glasses as AlO_4 tetrahedra and/or AlO_6 octahedra, depending on Al_2O_3/SrO ratio. If the ratio $Al_2O_3/SrO < 1$, only four coordinated aluminum ions AlO_4 are formed. For $Al_2O_3/SrO > 1$, AlO_6 groups are favored [10]. Some of the strontium aluminate glasses are used as photosensitive applications and thus are potential candidates for optical information storage devices. The research on the strontium alumino-borate glasses is essential as it finds application in many fields as described above. So to cater the need for probing, electron paramagnetic resonance (EPR) technique is a potential tool to study the lowest energy levels and hence the electronic state of the unpaired electrons of paramagnetic ions. FTIR and Raman studies are carried out to know the structural changes in the glass.

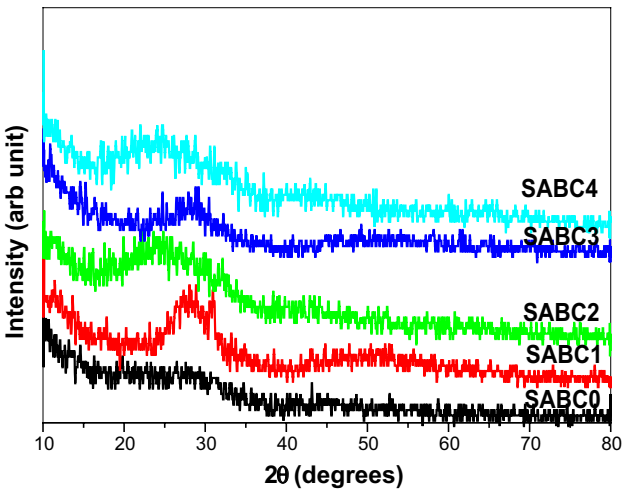

Fig. 2 X-ray diffraction pattern of SABC glasses

2 Experimental

The glass samples of the composition $(30-x)$ $SrO–xAl_2O_3–69.5B_2O_3–0.5CuO$, $0 \le x \le 15$ mol% (Table 1) in the present investigation are prepared by melt quenching method. Appropriate amounts of reagent grade of $SrCO_3$, Al_2O_3, H_3BO_3 and CuO powders were thoroughly mixed and taken in platinum crucible and then melted in an electrical furnace at the temperature ~ 1200 °C. The molten mixture is quenched to obtain blue-colored, transparent glass samples shown in Fig. 1. Phillips X-pert pro X-Ray diffractograms and Carl Zeiss model SEM were used to confirm the glassy nature. Density measurements were taken for these glasses. Optical absorption (UV–Vis) spectra were recorded using Shimadzu UV-1800 spectrophotometer in the region 200–1000 nm. ESR spectra are also recorded at room temperature on JOEL FE1X spectrometer operating X-band frequency with 100 kHz field modulation. JOBIN YVON HR800 (HORIBA) instrument is used to record Raman Spectra with (473 nm) a solid-state diode laser in the range 200–1600 cm^{-1}. A fine glass powder is used to record FTIR spectra on Shimadzu 8400S instrument in the 400–1600 cm^{-1} wavelength range. Glass transition temperature (T_g) of prepared glasses was determined using DSC thermograms, recorded on NETZSCH DSC 404F3 spectrometer with a heating rate of 10 K/min.

3 Result and discussion

3.1 XRD and SEM

Figure 2 shows the typical X-ray diffraction pattern for SABC glasses. There are no sharp peaks in the spectra, indicating that glasses are of amorphous nature. The SEM image of SABC2 glass shown in Fig. 3 revealed the clear smooth homogenous surface with no origination of clusters which also supports the amorphous nature.

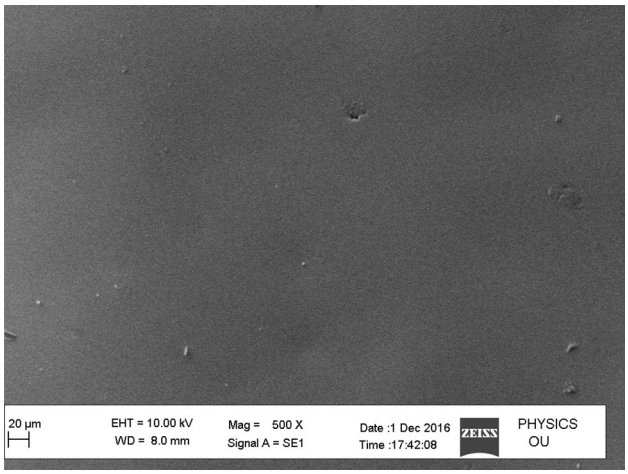

Fig. 3 SEM image of SABC 2 glass

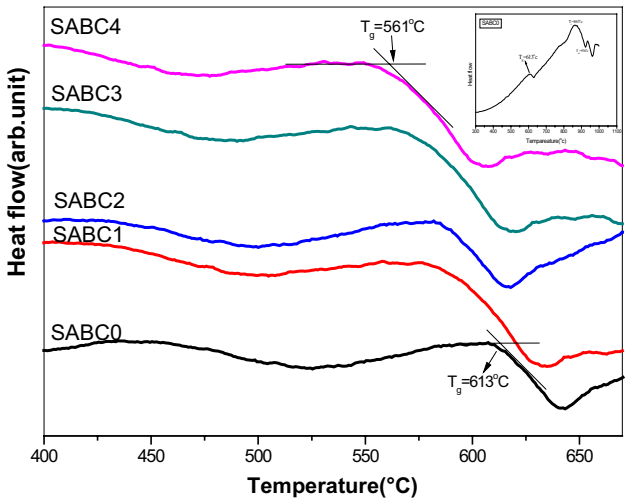

Fig. 4 DSC thermograms of SABC glasses

3.2 DSC studies

Figure 4 shows the decreasing T_g (from SABC0 to SABC4) with the increase in the Al_2O_3 content; this is often as a result of increase in the number of non-bridging oxygen (NBO) and the formation of AlO_4 tetrahedra and void space [11]. The increase in the concentration of Al_2O_3 in the SABC glass magnificently resulted in the blocking of network-modifying action of Sr^{2+} ions, thereby creating more BO_3 units [12].

3.3 Physical properties

Density measurements pave the way for understanding and analyzing the structure of a glassy network. From the literature survey, it is found that the density of the glass depends on modifier quantities like SrO, MgO, Na_2O, Al_2O_3, etc. [1, 3, 13]. Most of the research work on glasses includes density measurements employing Archimedes principle. Using density values, molar volume V_m is estimated [1, 14]. It is observed that the density values are decreasing from 2.705 to 2.451 g/cc with increasing Al_2O_3 from 5 to 15 mol% with decreasing equal amount of SrO content in the glass composition. The crystalline density of Al_2O_3 (3.95 g/cc) is much lower as compared to the density of SrO (4.7 g/cc) which might be one of the reasons behind the decrease in density when SrO is replaced by Al_2O_3. From the literature, it is understood that SrO acts as modifier and converts BO_3 units to BO_4 units. Al_2O_3 in the glass network generates AlO_4 tetrahedra and BO_3 units. The remaining aluminum reacts with CuO which leads to creation of the non-bridging oxygen (NBO) leading to more open structure [12, 15, 16]. This explains the increase in molar volume and decrease in density as shown in Fig. 5.

The average boron–boron separation $\langle d_{B-B} \rangle$ for SABC glasses is calculated using the relation [16] as

$$V_m^B = \frac{V_m}{2(1 - X_B)} \quad (1)$$

where X_B is the molar fraction of boron trioxide

$$\langle d_{B-B} \rangle = \left(\frac{V_m^B}{N_A} \right)^{\frac{1}{3}} \quad (2)$$

where N_A is 6.0221×10^{23} being the Avogadro number. The calculated values of $\langle d_{B-B} \rangle$ are given in Table 2.

Average boron–boron separation increases from 0.511 to 0.528 nm with increasing Al_2O_3 favoring increase in molar volume.

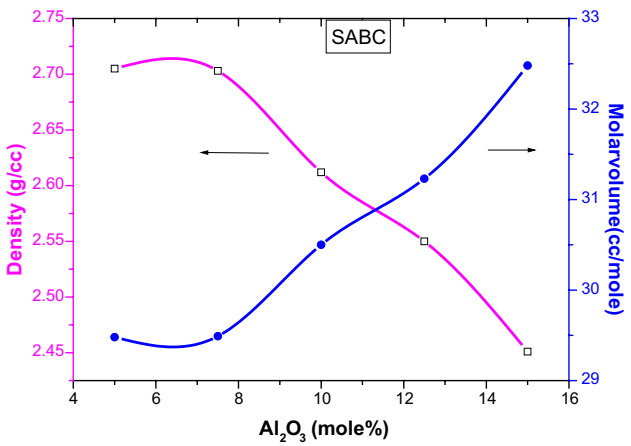

Fig. 5 Variation of density and molar volume with Al_2O_3 mol% of SABC glasses

Table 2 Physical properties of SABC glasses

Physical property parameters	$X=5$ mol%	$X=7.5$ mol%	$X=10$ mol%	$X=12.5$ mol%	$X=15$ mol%
Glass code	SABC0	SABC1	SABC2	SABC3	SABC4
Average molecular weight M (g)	79.784	79.742	79.701	79.659	79.618
Density ρ (g/cm^3) (±0.001)					
Experimental	2.705	2.703	2.612	2.550	2.451
Theoretical	2.682	2.605	2.531	2.459	2.389
Molar volume (cm^3/mole) (±0.01)	29.48	29.49	30.50	31.23	32.48
Oxygen packing density (mol/cm^3) (±0.01)	84.449	86.117	84.900	84.520	82.810
Ionic packing density (V_t)	0.617	0.626	0.615	0.609	0.594
Refractive index n_d	2.280	2.304	2.318	2.345	2.294
Molar refractivity R_m (cm^{-3})	17.193	17.384	18.090	18.736	19.358
Dielectric constant ε	5.198	5.308	5.373	5.499	5.262
Reflection loss R %	0.152	0.155	0.157	0.161	0.154
Transition metal ion concentration (Ni) 10^{21} (ions/cc) (±0.01)	10.21	10.20	9.87	9.64	9.27
Polaron radius (r_p) (A°) (±0.005)	2.20	2.21	2.23	2.25	2.28
Interionic distance (r_i) (A°)(±0.005)	5.46	5.47	5.53	5.56	5.63
Molar polarizability α_e (10^{-24} ions/cm^3) (±0.005)	6.82	6.89	7.17	7.43	7.68
Field strength (F) (10^{15} cm^{-2})	4.13	4.09	4.02	3.95	3.85
Average boron–boron distance (d_{B-B}) (nm)	0.511	0.512	0.517	0.521	0.528
Optical band gap (E_g) (eV) (±0.01)	3.47	3.37	3.31	3.20	3.41
Urbach energy (eV) (±0.001)	0.536	0.618	0.639	0.681	0.825
Optical basicity Λ_{th} (±0.001)	0.619	0.605	0.592	0.578	0.565

The refractive index (n_d) of BABC glasses has been computed by utilizing the relation given below [17]

$$\frac{(n_d^2-1)}{(n_d^2+2)} = 1-\sqrt{\frac{E_g}{20}} \tag{3}$$

where E_g is the energy band gap

Generally speaking, the increment is observed in a refractive index (n_d) from 2.375 to 2.501 in the present system as a result of the rise in the count of NBO.

From the refractive index (n_d) values, the dielectric constant (ε) was calculated by utilizing formula [17]

$$\varepsilon = n_d^2 \tag{4}$$

The molar refractivity R_M of the glass samples was evaluated using [16]

$$R_M = \left[\frac{n_d^2-1}{n_d^2+2}\right] * V_m \tag{5}$$

where n_d—refractive index, V_m—molar volume

Measurement of TM ion concentration per cc for host glasses provides information about the observed changes in its different properties. Hence, the measurement of TM ion concentration (N_i) is of great importance in the present case. It is being calculated by the formula [18]

$$N_i = \frac{N_A * X(\text{mol}\%) * d}{M} \tag{6}$$

where $X(\text{mol}\%)$ refers to a transition metal ion, d density, M average molecular weight.

The polaron radius (r_p) and interionic separation (r_i) are calculated through the following relation [18]

$$r_p = \frac{1}{2}\left(\frac{\pi}{6N_i}\right)^{\frac{1}{3}} \tag{7}$$

and

$$r_i = \left(\frac{1}{N_i}\right)^{\frac{1}{3}} \tag{8}$$

The electronic polarizability α_M for all the glass samples was evaluated using [17]

$$\alpha_e = \left(\frac{3}{4\pi N}\right) * R_M \tag{9}$$

The field strength is calculated using the oxidation number (Z) from the following formula [18]

$$F = \left(\frac{Z}{r_p^2}\right) \tag{10}$$

In general, polaron radius (r_p) is increasing and field strength is decreasing, showing the opposite trend which is clearly observed in the present work (Table 2). The value of r_p increases from 2.20 to 2.28 Å. This increment is attributed to the open structure caused by Cu^{2+} addition. Field strength (F) decreases also support the open structure, which resulted in an increase in molar volume [11]. The polaron radius (r_p) and interionic distance (r_i) results are in tune with each other. The polaron radius in all the glasses (SABC series) is less than the corresponding interionic distance which is in accordance with the usual prediction of the polaron theory that the polaron radius should be smaller than the site separation.

The theoretical optical basicity (Λ_{th}) is calculated using the relation mentioned below [16]

$$\Lambda_{th} = X_{BaO}\,\Lambda_{BaO} + X_{Al_2O_3}\Lambda_{Al_2O_3} + X_{B_2O_3}\Lambda_{B_2O_3} + X_{CuO}\Lambda_{CuO} \quad (11)$$

where X_{BaO}, $X_{Al_2O_3}$,$X_{B_2O_3}$,X_{CuO} are fractions of present oxides and Λ_{BaO}, $\Lambda_{Al_2O_3}$,$\Lambda_{B_2O_3}$, Λ_{CuO} are optical basicity values. The calculated values of optical basicity are given in Table 2. These values are decreasing from 0.619 to 0.565 with an increase in Al_2O_3 content. This trend shows the decreasing electron donar capability of oxide ions to the coordinate cations. The increase in the refractive index (n_d) and molar refractivity (R_m) indicates the presence of more polarizable electrons surrounding the oxygen. The variation of n_d and R_m with Al_2O_3 mol% is shown in Fig. 6.

3.4 EPR studies

Figure 7 shows EPR spectra of $(30-x)$ SrO–xAl_2O_3–$69.5B_2O_3$–0.5CuO glass systems. The general behavior of an ideal Cu^{2+} ion is to provide four parallel and four perpendicular hyperfine components satisfying the condition $(2I+1)$,

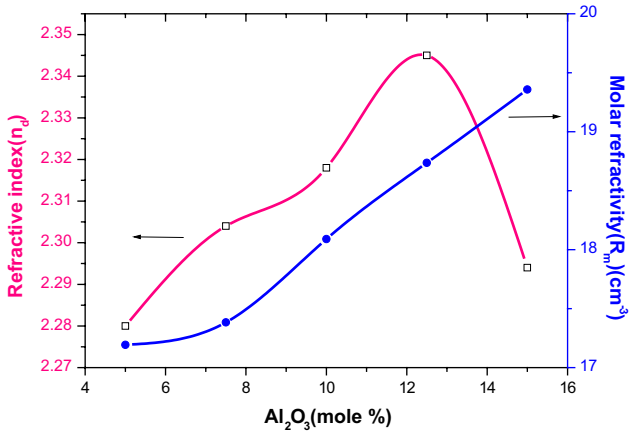

Fig. 6 Refractive index versus molar refractivity with Al_2O_3 mol% of SABC glasses

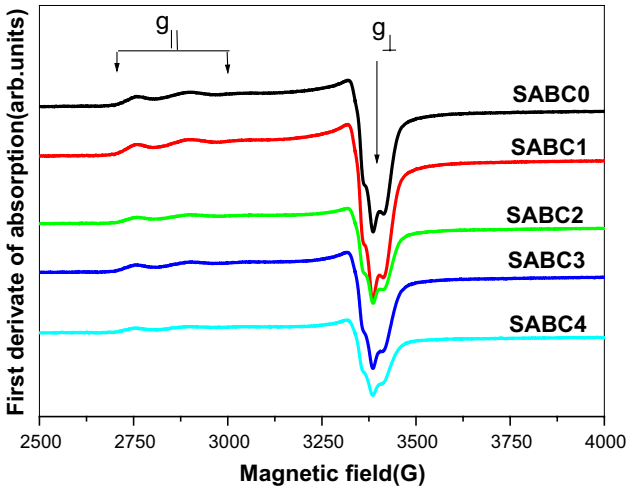

Fig. 7 EPR spectra of SABC glasses

where $I=3/2$ and $S=1/2$ for the Cu^{2+} ion. However, Cu^{2+} ion in glassy network has shown three feebly resolved parallel components while fourth being mixed with perpendicular component. Perpendicular hyperfine components are not well resolved. EPR signal intensity is modulated by the addition of Al_2O_3. This is clear from Fig. 7 that signal intensity is decreasing as moving from SABC0 to SABC4 glass sample. This shows that ligand field around Cu^{2+} ion is being greatly influenced by the addition of Al_2O_3. The presence of Al_2O_3 greatly hinders the hyperfine splitting.

Spin-Hamiltonian parameters are calculated using the expressions [19, 20]. $g_{\|}$ values varying between 2.335 and 2.340 are much greater than $g_{\perp}$ values (2.059–2.076) which in turn are greater when compared to free spin g value $g_e=2.0023$. The hyperfine splitting tensor is found be $A_{\|} > A_{\perp}$. From the above-mentioned data, it is clear that Cu^{2+} ions are located in tetragonally distorted octahedral site and the ground state of Cu^{2+} ions is $d_{x^2-y^2}$ orbital $^2B_{1g}$ state [20]. To fetch some more information regarding the concentration of Cu^{2+} ions that have actually participated in the resonance process, we calculated (N) values using the area under the EPR spectra and its values are given in Table 3. The following equation is used to obtain the N value [21]

$$N = \frac{A_x\left(\mathrm{Scan}_x\right)^2 G_{std}\left(H_m\right)_{std}\left(g_{std}\right)^2[S(s+1)]_{std}\left(P_{std}\right)^{\frac{1}{2}}}{A_{std}\left(Scan_{std}\right)^2 G_x\left(H_m\right)_x\left(g_x\right)^2[S(s+1)]_x\left(P_x\right)^{\frac{1}{2}}}[\mathrm{Std}] \quad (12)$$

The subscripts x and std represent corresponding quantities for SABC glasses and the reference ($CuSo_4{\cdot}5H_2O$). The magnetic susceptibility (χ) of Cu^{2+} ions has been calculated using the equation [21]

$$\chi = \frac{Ng^2\beta^2 J(J+1)}{3K_B T} \quad (13)$$

Table 3 Spin-Hamiltonian parameters and molecular orbital bonding coefficient values of the SABC glasses

Glass code	$g_{\parallel}$	$g_{\perp}$	α^2	β^2	β_1^2	ΔE_{xy} (cm^{-1})	$N \times 10^{21}$ (per kg)	$\chi \times 10^3$ m^3/kg
SABC0	2.334	2.061	0.7890	0.9747	0.8053	12674	1.57	1.90
SABC1	2.340	2.059	0.7972	0.9647	0.8041	12578	1.60	1.94
SABC2	2.340	2.061	0.7703	0.9983	0.8290	12531	1.79	2.06
SABC3	2.335	2.076	0.7965	0.9656	0.7873	12500	1.56	1.91
SABC4	2.338	2.065	0.7950	0.7917	0.9673	12547	1.57	2.51

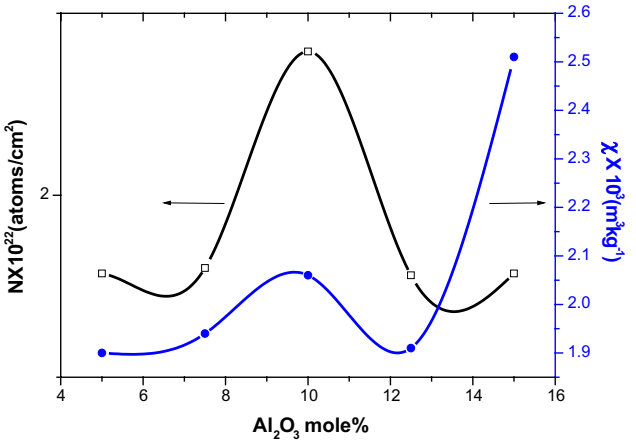

Fig. 8 Variation of spin concentration (*N*) and magnetic susceptibility (χ) with Al_2O_3 mol%

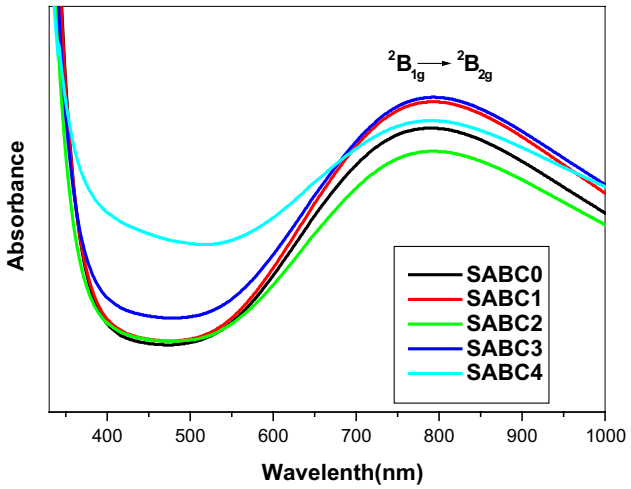

Fig. 9 Optical absorption spectra of SABC glasses

where *N* is the number of spins per kg, $J = 5/2$. Figure 8 shows the variation of *N* and χ with the Al_2O_3 (mol%) which is nonlinear.

3.5 Optical absorption spectra and energy band gap

The optical absorption spectra resulted due to the presence of Cu^{2+} ions in the glass system of SABC which has exhibited one broad absorption band (Fig. 9). This band is attributed to $^2B_{1g} \rightarrow {}^2B_{2g}$ transition. Using these spectra, the absorption coefficient 'α' can be measured as a function of frequency using the given formula [22]

$$\alpha(\nu) = \frac{A}{d} \times 2.303; \tag{14}$$

in the above equation, absorbance is represented by '*A*' at frequency *v* and '*d*' represents the thickness of the sample.

The indirect transitions are calculated using the relation [14]

$$\alpha(\nu) = b\left(h\nu - E_{\text{opt}}\right)^n / h\nu \tag{15}$$

where '*b*' is the energy-independent constant and in the above equation index *n* has different values, $n = 2$ and 1/2

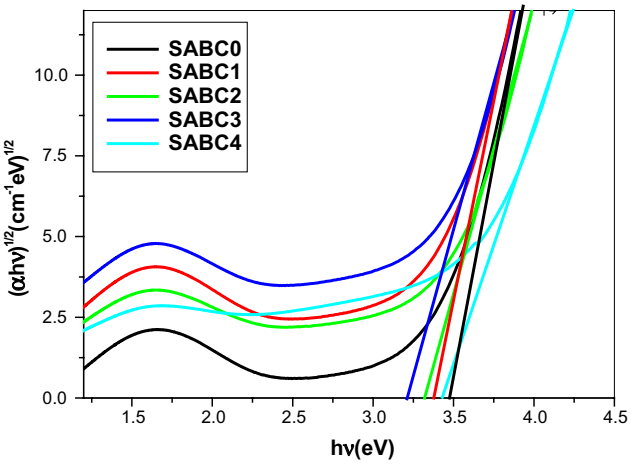

Fig. 10 Tauc plots of SABC glasses

for direct and indirect allowed transitions, respectively. The graph plotted for indirect transition is shown in Fig. 10. The optical band gap energy (E_{opt}) for indirect transitions is shown in Table 2 which is found to decrease with increasing Al_2O_3 due to an increment of NBO number in the glass sample. From the general definition, Urbach energy (ΔE) gives significant data about the density of energy states

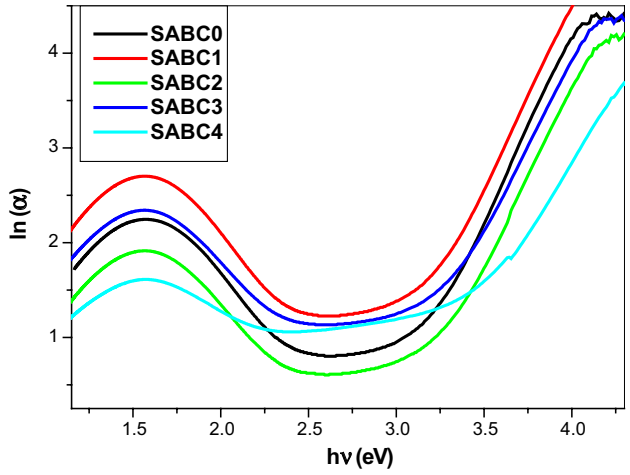

Fig. 11 Urbach plots of SABC glasses

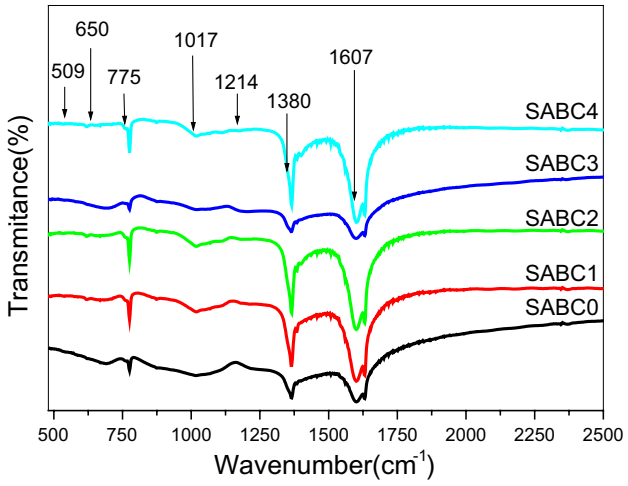

Fig. 12 FTIR spectra of SABC glasses

Table 4 FTIR band assignments of SABC glasses

Glass code					Band assignment	References
SABC0	SABC1	SABC2	SABC3	SABC4		
520	506	485	510	509	Vibration of metal cations (Sr^{2+}) and CuO bond vibrations.	[25, 26]
701	663	672	694	650	Bending vibration of B–O–B in BO_3 triangles	[27, 28]
781	775	775	775	775	BO_3–O–BO_4 bond bending vibration	[29, 30]
1013	1016	1010	1024	1017	B–O symmetric stretching of BO_4 units	[30, 31]
1210	1224	1225	1214	1208	B–O stretching vibration BO_3 units from phyro and orthoborate groups	[30, 32]
1395	1371	1364	1374	1380	B–O asymmetric vibrations in BO_3 and BO_2O units	[29, 31]
1608	1605	1602	1605	1607	Bending of O–H	[31, 33]

present in the optical band gap which is obtained from the plots drawn between *hv* versus ln(*α*) shown in Fig. 11.

Table 3 contains the peak position (ΔE_{xy}) obtained from optical absorption spectra (Fig. 9). This can be identified as the *d–d* transition band due to Cu^{2+} ion. The peak position is shifted toward higher wavelengths due to the ligand field around Cu^{2+} ion. Bonding parameters (α^2, β^2 and β_1^2) describing the bonding nature of bonding between the Cu^{2+} ion and its ligands are effectively evaluated by the data obtained from both EPR and optical absorption studies. The in-plane σ bonding represented by α^2 bonding between ligands (surrounding oxygen) and copper $d_{x^2-y^2}$ orbital is moderately ionic. The out-of-plane Π-bonding between ligands and copper $d_{xz,yz}$ orbital is represented by β^2 is found to be ionic, while β_1^2, the measure of in-plane Π-bonding with d_{xy} orbital, is mostly ionic in nature [19, 23]. Bonding parameters are given in Table 3. From these values, it may be concluded that Cu^{2+} ion is mostly in an ionic environment in the present SABC glass system [24].

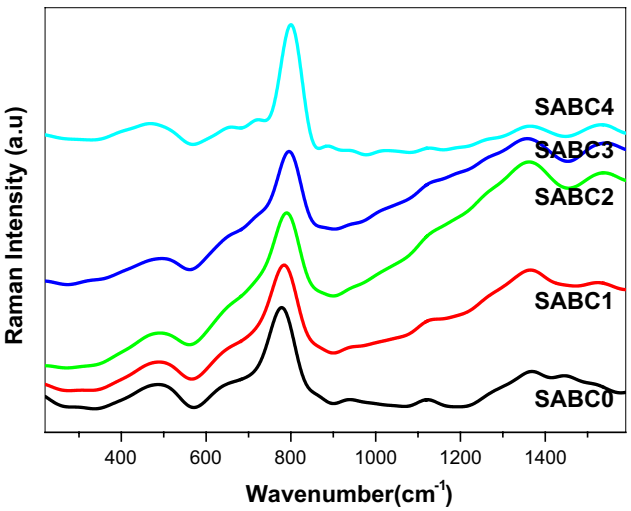

Fig. 13 Raman spectra of SABC glasses

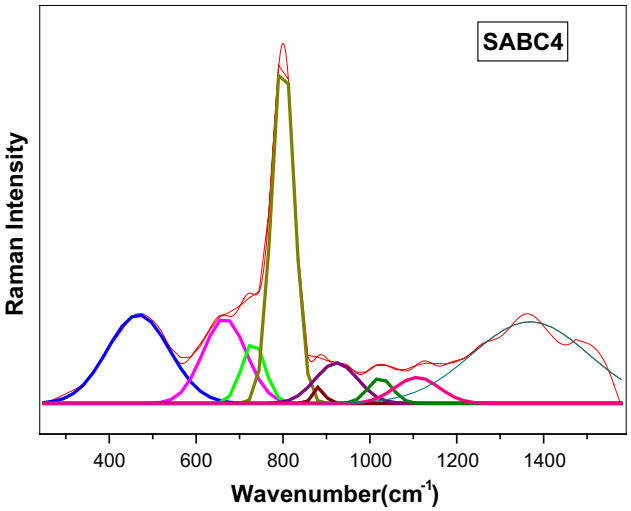

Fig. 14 Deconvoluted Raman spectra of SABC4 glass

3.6 FTIR studies

The FTIR spectra of SABC glasses revealed the presence of different vibrational units shown in Fig. 12. The FTIR transmission bands falling around ~ 509, ~ 650, ~ 775, ~ 1017, ~ 1214, ~ 1380, ~ 1608 cm^{-1} lying between wavenumbers 500–2500 cm^{-1} with their assignments are listed in Table 4. The present study shows that the quantitative evolution of these glass structures is enormously affected by the Al_2O_3 concentration. The band at ~ 509 cm^{-1} represents the metal cation, Sr^{2+} vibrations and also due to the transition metal ion Cu^{2+} [25, 26]. The FTIR band ~ 650 cm^{-1} is resulted due to the bending vibration of B-O-B in BO_3 triangles [27, 28]. The transmittance peak intensity is increasing for 775 cm^{-1} with Al_2O_3 mol percentage due to the BO_3–O–BO_4 bond bending vibrations [29, 30]. B–O symmetric stretching of BO_4 units is seen ~ 1017 cm^{-1}, while the wide band ~ 1214 cm^{-1} belongs to B–O stretching vibration BO_3 units from mixed borate groups like phyro- and orthoborates [31, 32]. The intensity of the sharp peak ~ 1380 cm^{-1} increases with Al_2O_3 increment due to B–O asymmetric vibrations in BO_3 and BO_2O units and indicates BO_3 increment with the increase in Al_2O_3 mol percentage [29, 31]. Another sharp band at ~ 1607 cm^{-1} is due to bending vibrations of O–H groups [31, 33].

3.7 Raman studies

Raman spectroscopy is extensively used to analyze the information about the structure and to explore the probable functional groups present in the glass. Raman spectra of SABC glasses are shown in Fig. 13, and deconvoluted Raman spectra of SABC4 glass are shown in Fig. 14. Raman peaks are explored from the deconvoluted graphs, and their assignments are listed in Table 5. The band seen ~ 468 cm^{-1} is due to the vibration of BO_4 isolated tetrahedra or isolated diborate groups [34, 35]. Raman band ~ 674 cm^{-1} is assigned as B-O-B stretching of metaborate rings [35, 36]. The sharp peak centered ~ 777 cm^{-1} is attributed to symmetric breathing vibrations of boroxol rings and also due to AlO_4 units [34, 36]. The band intensity is increasing with the addition of Al_2O_3 mol percentage, and shifting of the peak to higher wavelength is also observed. The band ~ 858 cm^{-1} represents [25, 34] the pyroborate groups, while the band ~ 942 cm^{-1} is due to the B–O bond stretching of orthoborate groups [25, 35]. A weak intensity peak at ~ 1028 cm^{-1} is assigned as diborate groups [34, 36]. The Raman peak at ~ 1261 cm^{-1} is due to B–O stretching in pyroborate units. The band at ~ 1362 cm^{-1} is generally due to B–O stretch in BO_4 units from varied borate groups [34, 38]. Raman peak

Table 5 Raman assignment for SABC glasses

Glass code					Band assignment	References
SABC0	SABC1	SABC2	SABC3	SABC4		
468	476	472	463	467	Vibration of BO_4 isolated tetrahedra/isolated diborate groups	[34, 35]
674	680	693	690	665	B–O–B stretching of metaborate ring	[35, 36]
777	784	790	796	791	Symmetric breathing vibrations of boroxol rings and AlO_4 Units	[34, 36]
858	884	880	889	800	Pyroborate groups	[25, 34]
942	985	977	958	923	B–O bond stretching of orthoborate group.	[25, 35]
1028	1039	1035	1012	1023	Diborate groups	[34, 36]
1128	1139	1126	1134	1123	Vibration of trigonal boron	[35, 37]
1261	1277	1223	1281	–	B–O stretching in pyroborate units	[36, 38]
1362	1374	1379	1358	1369	B–O stretch in BO_4 unit from varied borate group	[34, 38]
1437	1494	1514	1533	–	Stretching vibrations of BO_3 triangles with large segment of borate network	[39, 40]

at ~ 1437 cm^{-1} is attributed to stretching vibrations of BO_3 triangles with large segment of borate network [39, 40]. From Raman spectra analysis, it is clearly observed that the absence of the peak at 805 cm^{-1} concluded the absence of boroxol rings and existence of AlO_4 and BO_3 units observed at ~ 791 cm^{-1} and ~ 1533 cm^{-1}, respectively. The presence of pyroborate and orthoborate groups accepted the existence of non-bridging oxygen.

4 Conclusions

From the above investigations, the following conclusions are drawn:

1. XRD and SEM morphology confirms the glassy nature of the SABC glasses
2. Decreasing T_g with the increase in the Al_2O_3 content is an evidence for the increasing of NBO.
3. The decreasing density value for present glasses indicates the structural changes, due to Al_2O_3 increment. Al_2O_3 reacts with glass composition and from AlO_4 and BO_3 units with NBO. Using density and molar volume, OPD and ionic packing densities are calculated.
4. The Cu^{2+} ions in all the glass systems studied are in tetragonally distorted octahedral sites with $d_{x^2-y^2}$ orbital ($^2B_{1g}$) ground state. The spin-Hamiltonian parameters are influenced by the glass composition which may be attributed to the change in the ligand field strength around Cu^{2+}. From covalency parameters, it is concluded that α^2 is moderately ionic,β_1^2 is mostly ionic, and β^2 is ionic.
5. The optical absorption spectra of present glasses have shown a single broad peak assigned to $^2B_{1g} \rightarrow {}^2B_{2g}$ transition. Optical band gap and Urbach energies are calculated, and using this, data refractive index, polaron radius and molar refractivity are calculated. Decreasing values of optical band gap with increasing Al_2O_3 indicate the creation of NBO.
6. The FTIR and Raman studies confirmed the presence of BO_3 and BO_4 units in the glass network. The metal cation Sr^{2+} and Cu^{2+} vibrations are observed ~ 520 cm^{-1} in FTIR spectra. The sharp Raman peak ~ 777 cm^{-1} is attributed to symmetric breathing vibrations of boroxol rings and AlO_4 units.

Compliance with ethical standards

Conflict of interest The authors declare that they have no conflict of interest.

References

1. Mohan S, Thind KS, Sharma G (2007) Effect of Nd^{3+} concentration on the physical and absorption properties of sodium-lead-borate glasses. Braz J Phys 37:1306–1313. https://doi.org/10.1590/S0103-73320070008000019
2. Abdelghany AM, ElBatal HA (2013) Effect of TiO_2 doping and gamma ray irradiation on the properties of $SrO–B_2O_3$ glasses. J Non Cryst Solids 379:214–219. https://doi.org/10.1016/j.jnoncrysol.2013.08.020
3. Lim TY, Wagiran H, Hussin R, Hashim S, Saeed MA (2014) physical and optical properties of dysprosium ion doped strontium borate glasses. Phys B 451:63–67
4. Neel EAA, Chrzanowski W et al (2009) Doping of a high calcium oxide metaphosphate glass with titanium dioxide. J Non Cryst Solids 355:911–1000. https://doi.org/10.1016/j.jnoncrysol.2009.04.016
5. O'Connell K, Hanson M, O'Shea H, Boyd D (2015) Linear release of strontium ions from high borate glasses via lanthanide/alkali substitutions. J Non Cryst Solids 430:1–8. https://doi.org/10.1016/j.jnoncrysol.2015.09.017
6. Kaundal RS, Kaur S, Singh N (2010) Investigation of structural properties of lead strontium borate glasses for gamma-ray shielding applications. J Phys Chem Solids 71:1191–1195. https://doi.org/10.1016/j.jpcs.2010.04.016
7. Mohini GJ, Krishnamacharyulu N et al (2013) Studies on influence of aluminium ions on the bioactivity of B2O3–SiO_2–P_2O_5–Na_2O–CaO glass system by means of spectroscopic tudies. Appl Surf Sci 287:46–53. https://doi.org/10.1016/j.apsusc.2013.09.055
8. Abd El-Moneim A, Abd El-Daiem AM, Youssof IM (2003) Ultrasonic and structural studies on TiO_2-doped $CaO–Al_2O_3–B_2O_3$ glasses. Phys Status Solidi 199:192–201. https://doi.org/10.1002/pssa.200306651
9. Kim EA, Choi HW, Yang YS (2015) Effects ofAl_2O_3 on (1 – x)[$SrO–SiO_2–B_2O_3$]–xAl_2O_3 glass sealant for intermediate temperature solid oxide fuel cell. Ceram Int 41:14621–14626. https://doi.org/10.1016/j.ceramint.2015.07.182
10. Doweidar H (1998) Density-structure correlations in $Na_2O–Al_2O_3–SiO_2$ glasses. J Non Cryst Solids 240:55–65. https://doi.org/10.1016/S0022-3093(98)00719-4
11. Farouk M, Samir A, Metawe F, Elokr M (2013) Optical absorption and structural studies of bismuth borate glasses containing Er^{3+} ions. J Non Cryst Solids 371:14–21. https://doi.org/10.1016/j.jnoncrysol.2013.04.001
12. El-Alaily NA, Mohamed RM (2003) Effect of irradiation on some optical properties and density of lithium borate glass. Mater Sci Eng, B 98:193–203. https://doi.org/10.1016/S0921-5107(02)00587-1
13. Chanshetti UB, Shelke VA et al (2011) Density and molar volume studies of phosphate glasses. Phys Chem Technol 9:29–36. https://doi.org/10.2298/FUPCT1101029C
14. Chandra Sekhar K, Srinivas B et al (2017) The role of halides on a chromium ligand field in lead borate glasses. Mater Res Express 4:105203. https://doi.org/10.1088/2053-1591/aa8d7e
15. Ahmed MR, Sekhar KC, Hameed A et al (2018) Role of aluminum on the physical and spectroscopic properties of chromium-doped strontium alumino borate glasses. Int J Mod Phy B 32:1850095. https://doi.org/10.1142/s0217979218500959
16. Singh DP, Singh GP (2013) Conversion of covalent to ionic behavior of $Fe_2O_3–CeO_2–PbO–B_2O_3$ glasses for ionic and photonic application. J Alloy Compd 546:224–228. https://doi.org/10.1016/j.jallcom.2012.08.105
17. Pawar PP, Munishwar SR, Gedam RS (2016) Physical and optical properties of Dy^{3+}/Pr^{3+} Co-doped lithium borate

glasses for W-LED. J Alloys Compd 660:347–355. https://doi.org/10.1016/j.jallcom.2015.11.087
18. Chimalawong P, Kaewkhao J, Kedkaew C, Limsuwan P (2010) Optical and electronic polarizability investigation of Nd^{3+}-doped soda-lime silicate glasses. J Phys Chem Solidi 71:965–970. https://doi.org/10.1016/j.jpcs.2010.03.044
19. Shareefuddin Md, Jamal M, Narasimha Chary M (1996) Electron spin resonance and optical absorption spectra of Cu^{2+} ions in xNaI-(30 − x) Na_2O–70B_2O_3 glassesJ. Non Cryst Solids 201:95–101. https://doi.org/10.1016/0022-3093(95)00627-3
20. Hameed A, Ramadevudu G, Laksmisrinivas Rao S, Shareefuddin Md, Chary MN (2012) Electron paramagnetic resonance studies of Cu^{2+} and VO^{2+} spin probes in RO-Li_2O–Na_2O–K_2O–B_2O_3 (R = Zn, Mg, Sr and Ba) glass systems. New J Glass Ceram 2:51–58. https://doi.org/10.4236/njgc.2012.21008
21. SivaRamaiah G, LakshmanaRao J (2013) Electron spin resonance and optical absorption spectroscopic studies of Cu^{2+} ions in aluminium lead borate glasses. J Alloy Compd 551:399–404. https://doi.org/10.1016/j.jallcom.2012.10.023
22. Sekhar KC, Hameed A, Ramadevudu G, Narasimha Chary M, Shareefuddin Md (2017) Physical and spectroscopic studies on manganese ions in lead halo borate glasses. Mod Phys Lett B 16:1750180. https://doi.org/10.1142/S0217984917501809
23. Charadhar RPS, Yasoda B, Rao JL, Gopal NO (2006) Mixed alkali effect in Li_2O–Na_2O–B_2O_3 glasses containing CuO—an EPR and optical study. J Non Cryst Solids 352:3864–3871. https://doi.org/10.1016/j.jnoncrysol.2006.06.033
24. Ramadevudu G, Shareefuddin Md, Sunitha Bai N, Lakshmipathi Rao M, Narasimha Chary M (2000) Electron paramagnetic resonance and optical absorption studies of Cu^{2+} spin probe in MgO–Na_2O–B_2O_3 ternary glasses. J Non Cryst Solids 278:205–212. https://doi.org/10.1016/S0022-3093(00)00255-6
25. Gautam CR, Yadav AK (2013) Synthesis and optical investigations on (Ba, Sr)TiO_3 borosilicate glasses doped with La_2O_3. Opt Photonics J 3:1–7. https://doi.org/10.4236/opj.2013.34A001
26. Singh SP, Chakradhar RPS, Rao JL, Karmakar B (2013) Electron paramagnetic resonance, optical absorption and photoluminescence properties of Cu^{2+} ions in ZnO–Bi_2O_3–B_2O_3 glasses. J Magn Magn Mater 346:21–25. https://doi.org/10.1016/j.jmmm.2013.07.007
27. Narayana Reddy C, Veeranna Gowda VC, Sreekanth-Chakradhar RP (2008) Elastic properties and structural studies on lead–boro–vanadate glasses. J Non Cryst Solids 354:32–40. https://doi.org/10.1016/j.jnoncrysol.2007.07.011
28. Marimuthu K, Karunakaran RT, Surendra Babu S, Muralidharan G, Arumugam S, Jayasankar CK (2009) Structural and spectroscopic investigations on Eu^{3+}-doped alkali fluoroborate glasses. Solid State Sci 11:1297–1302. https://doi.org/10.1016/j.solidstatesciences.2009.04.011
29. Padmaja G, Kistaiah P (2009) Infrared and Raman spectroscopic studies on alkali borate glasses: evidence of mixed alkali effect. J Phys Chem A 113:2397–2404. https://doi.org/10.1021/jp809318e
30. Rajyasree Ch, Teja PMV, Murthy KVR, Rao DK (2011) Optical and other spectroscopic studies of lead, zinc bismuth borate glasses doped with CuO. Phys B 406:4366–4372. https://doi.org/10.1016/j.physb.2011.08.082
31. Taha TA, Abouhaswa AS (2018) Preparation and optical properties of borate glass doped with MnO_2. J Mater Sci: Mater Electron 29:8100–8106. https://doi.org/10.1007/s10854-018-8816-7
32. Naresh V, Buddhudu S (2012) Structural, thermal, dielectric and ac conductivity properties of lithium fluoro-borate optical glasses. Ceram Int 38:2325–2332. https://doi.org/10.1016/j.ceramint.2011.10.084
33. Limkitjaroenporn P, Kaewkhao J, Limsuwan P, Chewpraditkul W (2011) Physical, optical, structural and gamma-ray shielding properties of lead sodium borate glasses. J Phys Chem Solids 72:245–251. https://doi.org/10.1016/j.jpcs.2011.01.007
34. Pascuta P, Lungu R, Ardelean I (2010) FTIR and Raman spectroscopic investigation of some strontium–borate glasses doped with iron ions. J Mater Sci: Mater Electron 21:548–553. https://doi.org/10.1007/s10854-009-9955-7
35. Yadav AK, Singh P (2015) A review of the structures of oxide glasses by Raman spectroscopy. RSC Adv 5:67583–67609. http://pubs.rsc.org/ru/content/articlelanding/2015/ra/c5ra13043c
36. Santos CN, De Sousa Meneses D et al (2009) Structural, dielectric, and optical properties of yttrium calcium borate glasses. Appl Phys Lett 94:151901. https://doi.org/10.1063/1.3115796
37. Rejisha SR, Anjana PS, Gopakumar N, Santha N (2014) Synthesis and characterization of strontium and barium bismuth borate glass-ceramics. J Non Cryst Solids 388:68–74. https://doi.org/10.1016/j.jnoncrysol.2014.01.037
38. Ciceo-Lucacel R, Ardelean I (2007) FT-IR and Raman study of silver lead borate-based glasses. J Non Cryst Solids 353:2020–2024. https://doi.org/10.1016/j.jnoncrysol.2007.01.066
39. Nanda K, Berwal N et al (2015) Effect of doping of Nd^{3+} ions in BaO–TeO_2–B_2O_3 glasses: a vibrational and optical study. J Mol Struct 1088:147–154. https://doi.org/10.1016/j.molstruc.2015.02.021
40. Arunkumar S, Marimuthu K (2013) Concentration effect of Sm^{3+} ions in B_2O_3–PbO–PbF_2–Bi_2O_3–ZnO glasses—structural and luminescence investigations. J Alloys Compd 565:104–114. https://doi.org/10.1016/j.jallcom.2013.02.151